Materials Today Bio 16 (2022) 100379

Contents lists available at ScienceDirect

Materials Today Bio

journal homepage: www.journals.elsevier.com/materials-today-bio

Programmable molecular circuit discriminates multidrug-resistant bacteria

Xiaolin Hu [a,1], Weichao Qin [b,1], Rui Yuan [a], Liangliang Zhang [a], Liangting Wang [a], Ke Ding [c], Ruining Liu [a], Wanyun Huang [d], Hong Zhang [e,**], Yang Luo [b,a,f,*]

[a] Center of Smart Laboratory and Molecular Medicine, School of Medicine, Chongqing University, 174 Shazhengjie, Shapingba District, Chongqing, 400044, China
[b] Department of Clinical Laboratory, Jiangjin Hospital, Chongqing University, 725 Jiangzhou Road, Jiangjin District, Chongqing, 402260, China
[c] Department of Oncology, Jiangjin Hospital, Chongqing University, 725 Jiangzhou Road, Jiangjin District, Chongqing, 402260, China
[d] Life Science Laboratories, Biology Department, University of Massachusetts Amherst, 240 Thatcher Road, Amherst, MA, 01002, USA
[e] Department of Clinical Laboratory, The Second Hospital of Shandong University, 247 Beiyuan Street, Jinan, Shandong, 250033, China
[f] Department of Clinical Laboratory, Fuling Hospital, Chongqing University, 2 Gaosuntang Road, Fuling District, Chongqing, 408099, China

ARTICLE INFO

Keywords:
Aptamer
Bacteria
Detection
Enzyme
Infection
Nanomaterials

ABSTRACT

Recognizing multidrug-resistant (MDR) bacteria with high accuracy and precision from clinical samples has long been a difficulty. For reliable detection of MDR bacteria, we investigated a programmable molecular circuit called the Background-free isothermal circuital kit (BRICK). The BRICK method provides a near-zero background signal by integrating four inherent modules equivalent to the conversion, amplification, separation, and reading modules. Interference elimination is largely owing to a molybdenum disulfide nanosheets-based fluorescence nanoswitch and non-specific suppression mediated by molecular inhibitors. In less than 70 min, an accurate distinction of various MDR bacteria was achieved without bacterial lysis. The BRICK technique detected 6.73 CFU/mL of methicillin-resistant *Staphylococcus aureus* in clinical samples in a proof-of-concept trial. By simply reprogramming the sequence panel, such a high signal-to-noise characteristic has been proven in the four other superbugs. The proposed BRICK method can provide a universal platform for infection surveillance and environmental management thanks to its superior programmability.

1. Introduction

Multidrug-resistant (MDR) bacterial infection continues to be a substantial concern for worldwide public health, contributing to a significant rise in morbidity and mortality [1,2]. MDR bacteria evolve rapidly, accompanied by the overuse of antibiotics, and impose accessional burdens due to limited medication regimens [3,4]. Moreover, the sweeping and rapid spread of MDR bacteria is recognized as the dominant cause of serious infections [5,6]. Therefore, rapid and accurate detection of MDR bacteria in the early stages of infection plays a critical role in effectively preventing infection deterioration and community spread.

Bacterial culture accompanied by a susceptible test is still the most adopted methodology for determining MDR bacteria in routine clinical settings, attributed to its high accuracy and reliability. However, those redundant steps calling for over two days to achieve positive results have seriously hindered prompt clinical treatment decisions [7–9]. Instead, nucleic acid testing based on quantitative polymerase chain reaction (qPCR) of specific gene fragments takes significantly less time and has a much higher sensitivity, making it a viable tool for detecting MDR bacteria quickly. Nucleic acid testing-based fluorescence [10,11], electrochemistry [12,13], and colorimetry [14–16] biosensors have been constructed for the detection of MDR bacteria, and realized a single copy sensitivity. However, most existing designs require nucleic acid extraction procedures, leading to a risk of target contamination or possible degradation that may mislead to inaccurate results [17,18]. As a result, most molecular amplification approaches struggle to discriminate low-abundance MDR bacteria in clinical situations without lysis.

Molecular recognition elements that can anchor the bacterial surface protein with high specificity and affinity in a short time provide an innovative tool for signal conversion and break the bottleneck of lysis steps [19–21]. Among those molecular recognition elements ranging from antibodies to cellular wall-binding domain proteins, aptamers with

* Corresponding author. Department of Clinical Laboratory, Jiangjin Hospital, Chongqing University, 725 Jiangzhou Road, Jiangjin District, Chongqing, 402260, China.
** Corresponding author.
E-mail addresses: HongZ@sdu.edu.cn (H. Zhang), luoy@cqu.edu.cn (Y. Luo).
[1] These authors contributed equally to this work.

https://doi.org/10.1016/j.mtbio.2022.100379
Received 11 May 2022; Received in revised form 18 July 2022; Accepted 21 July 2022
Available online 11 August 2022

easy reprogramming potential and thermal stability have attracted increasing attention [22–25]. Therefore, various aptasensors conjugated with isothermal amplification technologies have been developed to allow rapid and direct determination of bacteria [26–28]. Among these amplification approaches, exponential amplification reaction (EXPAR) has been recognized as a practical tool to bolster the analytic sensitivity of existing approaches, whose amplification efficiency could reach 10^9 times within 30 min [29]. However, abundant false-positive results have been widely reported for conventional EXPAR strategies owing to serious non-specific amplification derived from inter-template hybridization [30–32]. Innovatory attempts, such as improved sequence design [30,33,34] and template sealer [35–37], had made significant progress in partially reducing these non-specific amplicons by delaying target-independent amplification, but still suffered from the residue that could generate background signals. Therefore, eliminating residual errors would facilitate accurate discrimination of MDR bacteria, especially at low concentrations (less than 100 CFU/mL).

Molybdenum disulfide (MoS_2) has been given wide attention due to its 2D layer structure analogous to graphene [38]. Previous research has revealed that MoS_2 nanosheets could strongly adsorb single-stranded DNA (ssDNA) by van der Waals forces between nucleobases and the basal plane of MoS_2 nanosheets [39,40]. The fluorescence quenching capabilities of MoS_2 enable those fluorescent ssDNA probes loaded onto the MoS_2 nanosheets to construct a convenient biosensing strategy, which could correspond to the complementary ssDNA using an "off--to-on" signal readout mechanism [41–44]. Inspired by these previous reports, we proposed a background-free isothermal circuital kit (BRICK) for the reliable discrimination of MDR bacteria. Low background interference was supported by a synergistic effect between two mechanisms: (i) molecular inhibitors reduced non-specific amplification vastly; (ii) MoS_2 nanosheets physically absorbed the remaining few non-specific amplicons. Results showed that the proposed BRICK approach delivered a near-zero background noise and high sensitivity (detection limit: 6.73 CFU/mL). Additionally, accurate discrimination of methicillin-resistant *Staphylococcus aureus* (MRSA) from other bacteria in clinical samples could be finished within 70 min. As demonstrated by the experiments detecting several other MDR bacteria, we have further proven the programmability of the BRICK approach by simply designing specific nucleic acid probes.

2. Results and discussion

2.1. Design rationale of the BRICK strategy

The operation of the BRICK strategy relied on the conversion, amplification, separation, and reading modules (Fig. 1A). The introduction of targets uncoiled the aptamer-blocker duplex modified on the surface of aptamer-functionalized magnetic beads (AptMBs), by which the blockers could be collected magnetically to realize signal conversion from bacteria to nucleic acid (Fig. 1B). Then the dissociative blockers hybridized with an EXPAR template to generate incomplete duplexes, and triggered the amplification module. Notably, the EXPAR template consisted of two identical sequences complementary to the blockers and 9-nt sequences, including the endonuclease recognition site (CTCAG) and interval sequence (ACTT). Hence, a new blocker was produced through the catalysis of endonuclease and polymerase, by which exponential amplification was realized (Fig. 1C).

To strike off background signals generated from non-specific amplification, we designed an "off-to-on" fluorescent nanoswitch based on the adsorption property of MoS_2 nanosheets and hybridization-mediated ssDNA detachment from the surface of MoS_2 nanosheets. The adsorption property was primarily activated, and the nanoswitch was turned off to produce a near-zero background signal. Notably, any non-specific amplicons from the inter-template hybridization of EXPAR also yielded a nearly signal increase, where the fluorescent nanoswitch remained "off" status. We are delighted to observe that MDR bacteria-driven specific EXPAR generated massive blockers, which finally exceeded the maximum absorption ability of MoS_2 nanosheets for ssDNA. Therefore, the fluorescent nanoswitch was turned on in the presence of target MDR bacteria (Fig. 1D).

2.2. Feasibility of the BRICK strategy

By taking MRSA as an analytical model in a proof-of-concept experiment, we first synthesized and characterized MRSA-specific AptMBs. Scanning electron microscopy (SEM) and dynamic light scattering (DLS) analysis showed that AptMBs were uniform, and had a diameter ranging from 0.355 μm to 2.244 μm (Fig. 2A and Fig. S1). The energy spectrum data revealed that AptMBs contained both iron and oxygen elements that

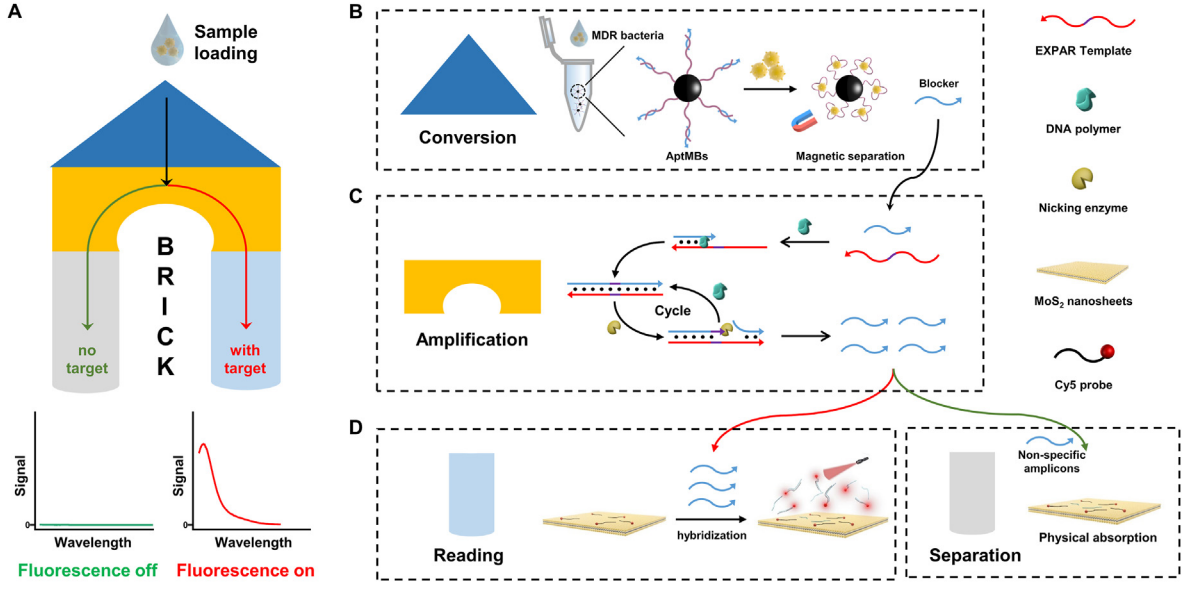

Fig. 1. (A) Schematic illustration of the mechanism of BRICK assay for MDR bacteria detection. Working mechanisms of the (B) Conversion module, (C) Amplification module and (D) Separation and reading module.

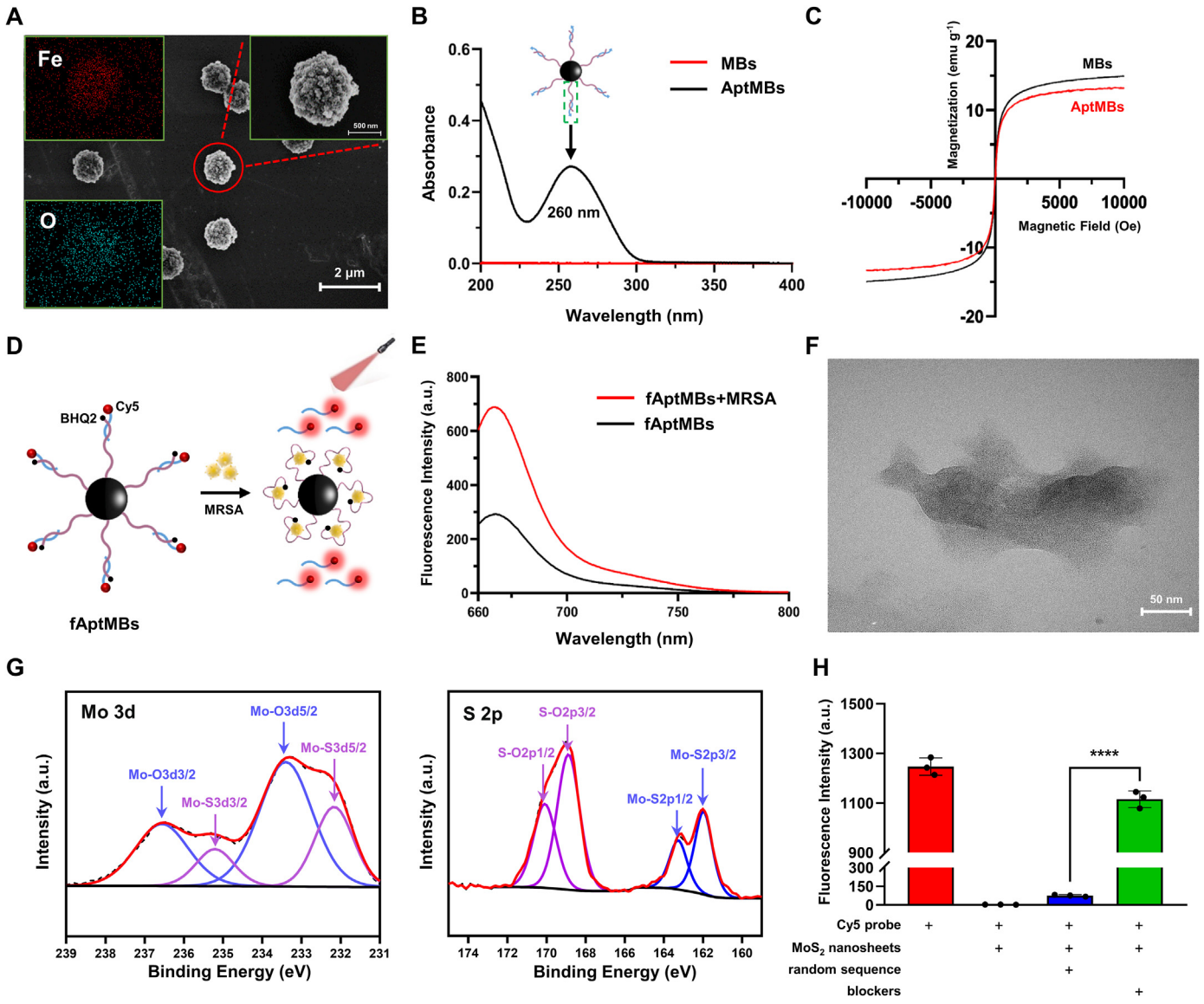

Fig. 2. Characterization of AptMBs and MoS_2 nanosheets. (A) SEM image of AptMBs (scale bar: 2 μm). The left insert is element energy spectra, and the right insert is an SEM image of the single AptMBs (scale bar: 500 nm). (B) The UV absorption spectrum and (C) Magnetic hysteresis loop of AptMBs and MBs. (D) The schematic diagram of the conversion efficiency verification. Fluorescence exhibited "off" resulting from BHQ2-labeled aptamers and turned "on" when cy5-label blockers were replaced with the addition of MRSA. (E) Fluorescence spectra of fAptMBs with the absence (black) and presence (red) of MRSA. (F) TEM image of MoS_2 nanosheets (scale bar: 50 nm). (G) XPS spectra of MoS_2 nanosheets: Mo 3d (left), S 2p (right). (H) Fluorescence intensity of the cy5 probe, cy5 probe + MoS_2 nanosheets, cy5 probe + MoS_2 nanosheets + random sequence and cy5 probe + MoS_2 nanosheets + blockers. The concentration of all the sequences was 100 nM, while the concentration of MoS_2 nanosheets was 5 μg/mL. Error bars represent standard derivations of three independent replicates. ****$p < 0.0001$. (For interpretation of the references to colour in this figure legend, the reader is referred to the Web version of this article.)

reflected the appearance of ferric oxide particles (Fig. 2A, insert). The UV absorption spectrum of AptMBs further demonstrated a remarkable peak at 260 nm responsible for an aptamer-blocker duplex on the surface-modified AptMBs, suggesting a successful connection between magnetic beads (MBs) and nucleic acid probe (Fig. 2B). Meanwhile, AptMBs had prominent superparamagnetic properties with a saturation magnetization of 12.5 emu/g, and no apparent alteration was discovered even after the assembly of the aptamer-blocker duplex on the AptMBs (Fig. 2C).

The unlocking of blockers was a prerequisite for initiating the amplification module in the presence of the MRSA. Thus, we verified the replacement ability of MRSA by constructing fluorescent AptMBs (fAptMBs) on which BHQ2-labeled aptamers and cy5-labeled blockers were assembled. The results showed a visible recovery of peak fluorescence intensity from 292.9 a.u. to 688.3 a.u. with the addition of MRSA, suggesting that the blockers had been successfully released (Fig. 2D–E). In evaluating the feasibility of EXPAR, PAGE analysis demonstrated a bright ~18 nt long blocker band in lane 5, indicating successful amplification (Fig. S2).

MoS_2 nanosheets-mediated background-free readout was one of the critical requirements for enhancing the analytical sensitivity. Therefore, we evaluated the synthesized MoS_2 nanosheets by transmission electron microscopy (TEM) and X-ray photoelectron spectroscopy (XPS). TEM images clearly showed the layered structure (Fig. 2F), and XPS spectra confirmed the existence of the Mo–S bond in the synthesized material (Fig. S3). Meanwhile, two characteristic Mo 3d spectra peaks at 232 eV and 235 eV corresponding to Mo $3d_{5/2}$ and Mo $3d_{3/2}$ orbitals, and S 2p spectra peaks at 162 eV and 163 eV corresponding to the S $2p_{3/2}$ and S $2p_{1/2}$ orbitals were also observed, respectively (Fig. 2G). After that, we verified the response efficiency of the fluorescent nanoswitch by

recording the recovery of peak fluorescence intensity. The results showed negligible background fluorescence intensity (black line) when only a primary cy5-terminated ssDNA probe existed on the surface of MoS_2 nanosheets. Significant fluorescence recovery with an efficiency of ~89.5% (mean peak intensity ratio: 1116/1247) was observed after the addition of blockers (green line), while a random sequence (purple line) yielded only ~6% (mean peak intensity ratio: 75.1/1247) (Fig. 2H).

2.3. Verification of background-free reading

Considering that non-specific amplification is inevitable in most conventional EXPAR systems, we carefully validated the specificity of the proposed BRICK approach. In our preliminary experiment performing a classical EXPAR test, non-specific amplicons could be observed in the PAGE image (Fig. S2, lane 4). Despite that the introduction of molecular inhibitors such as TMAC could alter the melting temperature (Tm) value of DNA and eliminate the base composition-dependent DNA transition temperature to postpone the non-specific reaction to some extent, a few amplicons could still be observed. Fortunately, we overcame the interference of those leaked amplicons by using the absorption function of the MoS_2 nanosheets so that the fluorescent nanoswitch remained "off" status (Fig. 3A).

We first evaluated the feasibility of the above mechanism. As shown in Fig. 3B, PAGE analysis demonstrated that an ~18 nt long blocker band representing non-specific leakage was observed in lane 3, and dimmed along with the addition of TMAC, demonstrating successful inhibition of target-independent amplification (lane 4). Additionally, target-dependent amplification was partially inhibited (lanes 5 and 6). Furthermore, we evaluated the output signals of these amplicons ranging from lane 3 to lane 6. Fig. 3C demonstrated that both non-specific and specific amplifications could be inhibited with the intervention of TMAC (EXPAR products of lanes 4 and 6).

To achieve a maximum signal-to-noise ratio, we first optimized the blocker sequence and reaction conditions. According to the relevant references [45,46], we designed three blockers and identified blocker 3 with the optimal substitution efficiency (Fig. S4). After that, the non-specific inhibitory effect of TMAC was first assessed by qPCR, and a time delay in the non-specific reaction was noted along with the increased TMAC concentration (Fig. 3D), which was also confirmed in the PAGE analysis (Fig. S5). We also verified the efficiency of target-dependent EXPAR to ensure that specific amplicons could be generated. The results demonstrated that reduced specific amplicons were observed when the concentration of TMAC was higher than 200 mM (Fig. S6), and PAGE analysis further confirmed the conclusion (Fig. S7). Additionally, we evaluated the influence of reaction time on signal reading. The results demonstrated that the peak fluorescence intensity increased with time, and reached its maximum by 60 min (Fig. S8). Thus, the optimal concentration of 200 mM and reaction time of 60 min were chosen in the following experiments. Finally, we optimized the concentration of MoS_2 nanosheets to realize the removal of residual leakage to obtain the best signal-to-noise ratio. Fig. 3E demonstrated that the fluorescence intensity of the noise group decreased more significantly than the signal group with the increase of MoS_2 nanosheets concentration and approached zero at 5 μg/mL, indicating that almost all cy5 probes were absorbed on the MoS_2 nanosheets. An over 300-fold signal-to-noise ratio was achieved when the concentration of MoS_2 nanosheets reached 5 μg/mL (Fig. S9). Notably, the reduced signal-to-noise ratio was observed when the concentration of MoS_2 nanosheets was higher than 5 μg/mL, which may be attributed to excessive absorption of specific amplicons.

2.4. Operating performance of the BRICK strategy

We evaluated the operating performance of the BRICK strategy under the optimal conditions during MRSA detection. The sensitivity analysis showed that peak fluorescence intensity increased proportionally to the increased MRSA concentration from 10 to 10^6 CFU/mL (Fig. 4A). A satisfactory linear correlation was achieved, and the logarithm

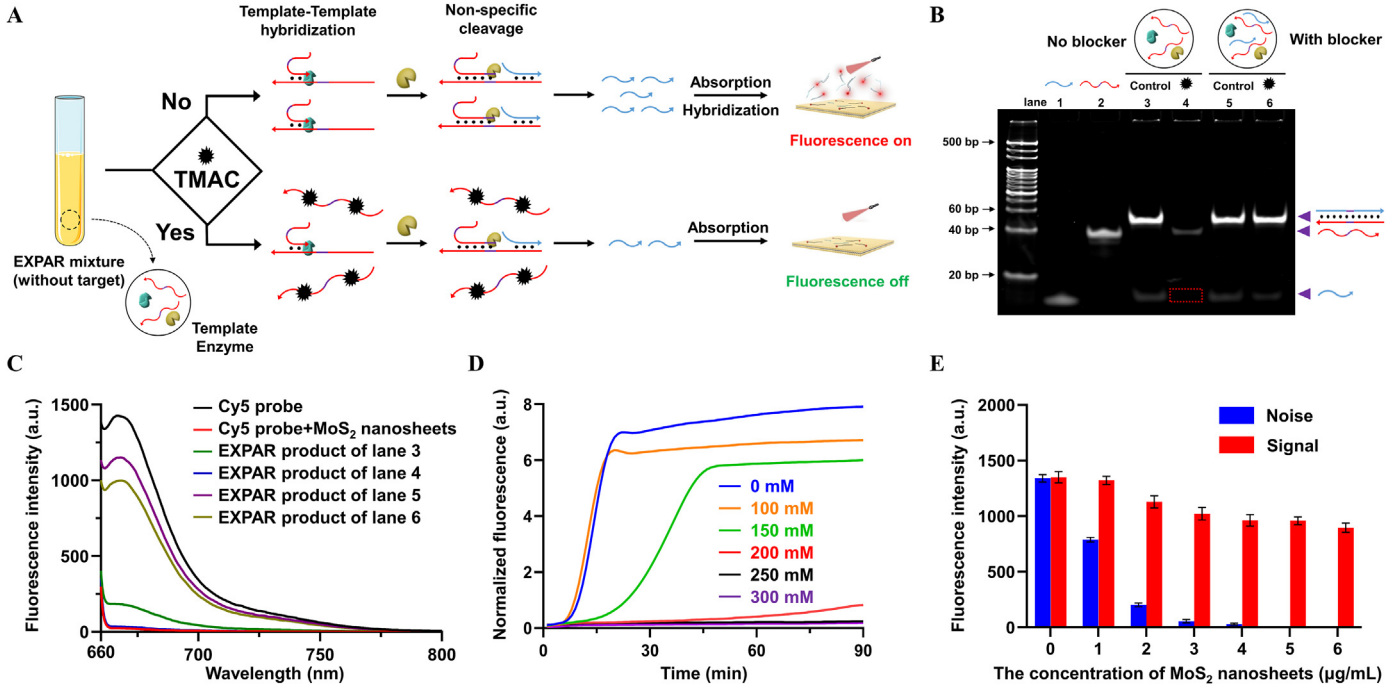

Fig. 3. Verification of background-free reading. (A) the mechanism of background signal inhibitions. (B) PAGE analysis of the inhibitory effect of TMAC. (C) Fluorescence spectra of the cy5 probe, cy5 probe + MoS_2 nanosheets, and after adding EXPAR products (lane 3), EXPAR products (lane 4), EXPAR products (lane 5), EXPAR products (lane 6) to the reading module. (D) qPCR analysis of non-specific inhibition with a series of concentrations of TMAC (0, 100, 150, 200, 250, and 300 mM). (E) the optimization of the working concentration of MoS_2 nanosheets. Error bars represent standard derivations of three independent replicates.

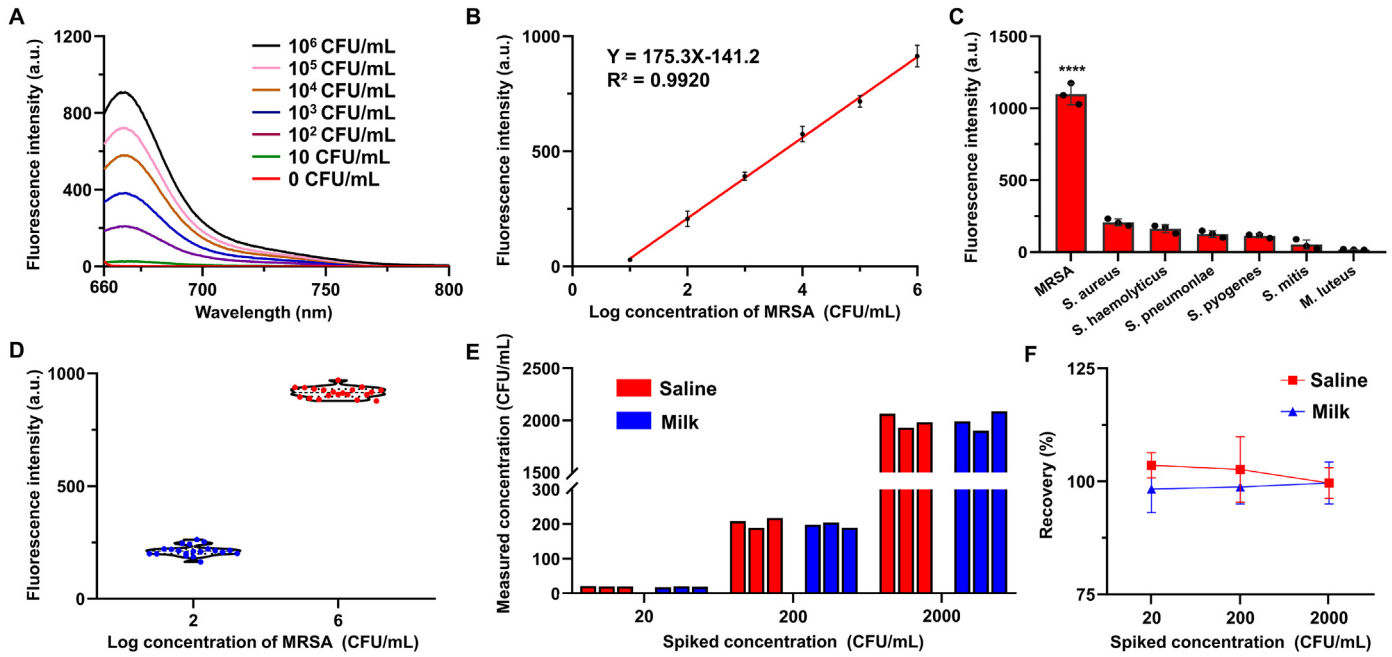

Fig. 4. Performance of the BRICK strategy. (A) Fluorescence spectra after adding the following series of concentrations of MRSA (0, 10^1, 10^2, 10^3, 10^4, 10^5, 10^6 CFU/mL, respectively). (B) Linear correlation between the fluorescence peak and the logarithm concentration of MRSA. Concentration of MoS_2 nanosheets: 5 μg/mL; cy5 probe: 100 nM. (C) Responses of fluorescence peak for MRSA, *S. aureus*, *S. haemolyticus*, *S. pneumoniae*, *S. pyogenes*, *S. mitis*, and *M. luteus*, respectively. The concentration of each bacterium is 10^6 CFU/mL, $^{****}p < 0.0001$. (D) Reproducibility of the peak fluorescence intensity among 20 independent replications using 10^2 and 10^6 CFU/mL of MRSA. (E) Measured concentrations and (F) corresponding recoveries after spiking saline and milk samples with a series of concentrations of MRSA (20, 200, 2000 CFU/mL) into the BRICK strategy. Error bars represent standard derivations of three independent replicates.

concentration of MRSA could be fitted as Y = 175.3X - 141.2, where Y presented the peak fluorescence intensities and X denoted the logarithm concentration of MRSA (correlation coefficient of 0.9920). Meanwhile, a detection limit of 6.73 CFU/mL was obtained by calculating the mean fluorescence intensity of 10 negative samples plus 3 standard deviations (SD) (Fig. 4B and Fig. S10). The specificity of the BRICK approach was verified by detecting several other bacterial strains, including *Staphylococcus aureus* (*S. aureus*), *Staphylococcus haemolyticus* (*S. haemolyticus*), *Streptococcus pneumoniae* (*S. pneumoniae*), *Streptococcus pyogenes* (*S. pyogenes*), *Streptococcus mitis* (*S. mitis*), and *Micrococcus luteus* (*M. luteus*). The results showed that MRSA yielded significantly higher signals than those from other bacteria ($p < 0.0001$) (Fig. 4C).

The reproducibility of this circuit was tested by measuring 20 duplicates of cultured MRSA with both high (10^6 CFU/mL) and low (10^2 CFU/mL) concentrations. Analogous output signals showed that both concentrations had relative standard deviations of less than 11% (Fig. 4D). Consistently, all measured values were in the interval range of $\overline{X} \pm 3$ SD with the classical Westgard multi-rule quality control method, suggesting that the BRICK assay provided acceptable reproduction capability (Fig. S11). To identify the practical applicability of the BRICK approach in real sample detection, a standard addition experiment in saline and milk was adopted. The results demonstrated that the recoveries of the spiked MRSA ranged from 99.64% to 103.55% in saline and 98.33%–99.63% in milk (Fig. 4E and F).

2.5. Feasibility validation in clinical sample detection

We further verified the discrimination capability of the BRICK strategy in 10 clinical MRSA infection samples (7 positives and 3 negatives) by comparing it with the conventional culture method. The colony counting results demonstrated that positive samples clearly showed bacterial proliferation on culture plates (Sample 1–7), while no proliferation was observed for those negative samples (Sample 8–10) (Fig. 5A). Similarly, significant signal variations between clinical positive and negative samples were validated in the BRICK approach (Fig. 5B). Furthermore, a threshold was determined to detect those negative and positive samples by calculating the average value of negative samples plus 3 SD (95% confidence level). The counting results of the proposed BRICK strategy achieved a 100% accuracy when compared with the culture method, and the receiver operating characteristic curves (ROC) indicated a high predictive power with an area under the curve (AUC) of 1.00 (95% confidence level: 1.00 to 1.00, $p < 0.0001$) (Fig. 5C–E).

2.6. Programmability validation by detecting other MDR bacteria

To validate the potential for recognizing other MDR bacteria, we developed four BRICK formats corresponding to MDR *A. baumannii*, *M. tuberculosis*, *P. aeruginosa,* and *E. coli* by reprogramming distinctive sequences, respectively (including aptamer, blocker, template, and probe). The working process of the BRICK system was illustrated in Fig. 6A, and the detection of MDR bacteria could be completed in less than 70 min. Considering the working mechanism of TMAC, the change of hybridization temperatures between blockers and templates attributed to sequence reprogramming may result in decreased suppression efficiency. (*A. baumannii*: 56.6°C, *M. tuberculosis*: 54.8°C, *P. aeruginosa*: 66.4°C, and *E. coli*: 60.6°C). Similarly, PAGE and qPCR analyses were conducted to evaluate the inhibition of non-specific amplification. PAGE images of four BRICK formats exhibited that no products were presented for non-specific amplification (Fig. 6C, lane 3). Additionally, the qPCR analysis demonstrated the occurrence of EXPAR with the addition of corresponding blockers (Fig. 6D).

The specificity of four BRICK formats was analyzed by cross-validating the clinical samples. We added four different types of MDR bacteria into all the BRICK formats and read the induced fluorescence intensities. The results showed that the activities of the BRICK format could only be independently activated by the corresponding MDR bacteria, respectively (Fig. 6B). Furthermore, samples containing a series of concentrations of MDR bacteria (0, 10^2, 10^4,10^6 CFU/mL) were input into corresponding BRICK formats to evaluate the analytical performance. Negligible fluorescent signals were collected from the four BRICK

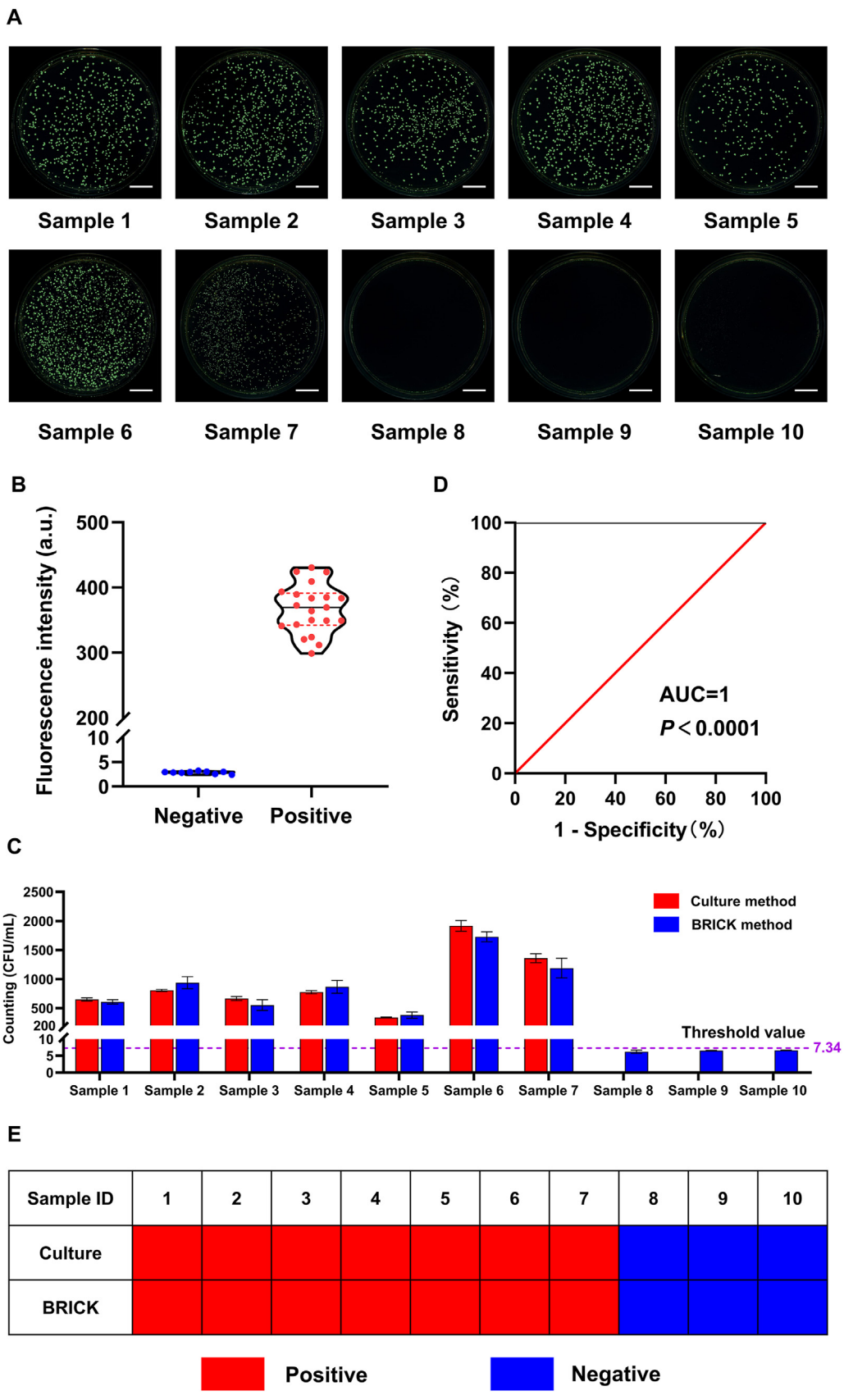

Fig. 5. Identification of MRSA with the culture method and BRICK method in clinical samples. (A) Colony counting results in culture plates (scale bar: 2 cm). (B) The measured fluorescence intensity using the BRICK approach in detecting clinically negative and positive samples. (C) 7 positive and 3 negative clinical samples were quantified by the culture method and BRICK method, respectively. The threshold value was defined as the mean value of clinical negative samples plus 3 SD (95% confidence level). Error bars represent standard derivations of three independent replicates. (D) Receiver operator characteristic (ROC) curve of MRSA positive versus negative. (E) Summary of test results: blue boxes indicated that MRSA was not detected in negative samples, and red boxes show that the MRSA was tested positive. (For interpretation of the references to colour in this figure legend, the reader is referred to the Web version of this article.)

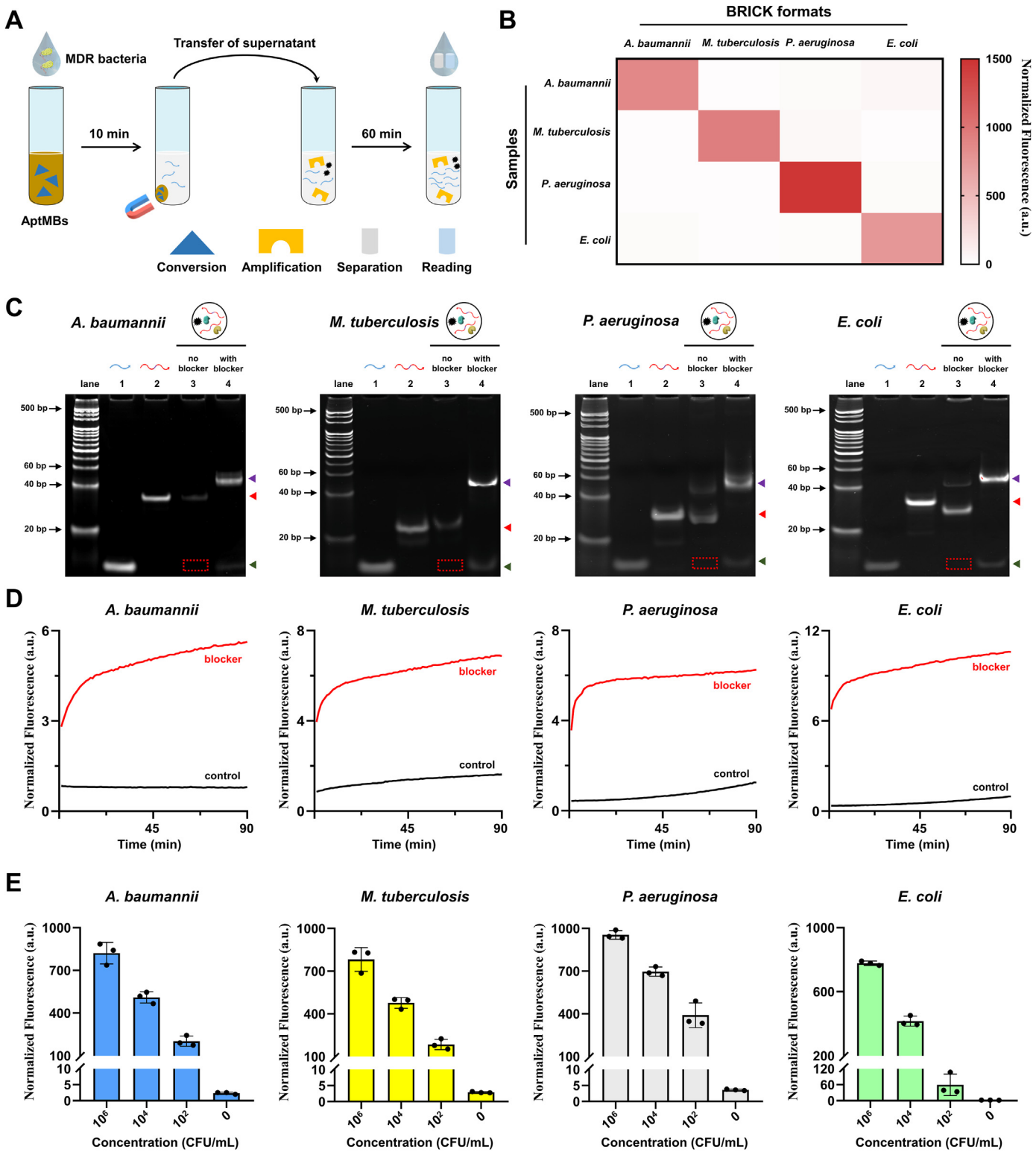

Fig. 6. Development of the universal BRICK platform. (A) The process of the BRICK system in MDR bacteria detection. The whole process could be completed within 70 min. (B) Multiplexed detection of MDR *A. baumannii*, *M. tuberculosis*, *P. aeruginosa,* and *E. coli* with the corresponding BRICK systems. (C) PAGE analysis of different MDR bacteria. Lane 1: 1 μM blocker; lane 2: 1 μM template; lane 3: EXPAR products with the absence of blocker; lane 4: EXPAR products with the presence of blockers. Green arrows: blocker bands, red arrows: template bands, and purple arrows: blocker-template duplex bands. (D) qPCR analysis of different MDR bacteria with and without blocker. (E) Response of four BRICK systems in detecting a series of concentrations of corresponding MDR bacteria (0, 10^2, 10^4, 10^6 CFU/mL). Error bars represent standard derivations of three independent replicates. (For interpretation of the references to colour in this figure legend, the reader is referred to the Web version of this article.)

formats without target bacteria. Comparatively, the fluorescence intensity recovered proportionally to the increase in bacterial concentration (Fig. 6E).

Although the proposed circuit has the potential to be a robust and universal platform for MDR bacteria compared to other MDR bacterial detection strategies (Table S1), it still needs additional improvement. In particular, BRICK could only detect a single bacterium once in the current format, which may limit its applications in analyzing complicated samples. We are endeavoring to introduce multiple fluorophores and integrate microfluidic chips to improve the capability of simultaneous detection of multiple MDR bacteria.

3. Conclusion

In summary, we created the background-free isothermal circuital kit (BRICK), a programmable molecular circuit for sensitive and accurate MDR bacteria differentiation in clinical samples. The superiority of the proposed BRICK approach mainly relies on its extremely low background interference, which was supported by a synergistic effect of two aspects: (i) TMAC could reduce non-specific amplification vastly; (ii) MoS_2 nanosheets physically absorb the remaining few non-specific amplicons. The BRICK approach revealed a high resolution in identifying low quantities of MDR with a detection limit as low as 6.73 CFU/mL using MRSA as a proof-of-concept experiment, and both the experimental and clinical sample analyses supported its resilience.

Empowered with convenient sequence reprogramming potential, our circuit had proven to be a versatile tool for identifying a wide range of MDR bacteria. Notably, most circuit modules are identical for all targeted MDR bacteria, therefore avoiding complicated optimization processes, highlighting its prospect as a robust and straightforward universal platform for pathogenic microorganism identification.

4. Materials and methods

4.1. Reagents

All the sequences listed in Table S2 were synthesized and purified by Sangon Biotech Co., Ltd (Shanghai, China) with high-performance liquid chromatography (HPLC). Nt. BstNBI endonuclease (10,000 U/mL), Vent® (exo-) DNA polymerase (2000 U/mL), dNTP, NEBuffer 3.1 (100 mM NaCl, 50 mM Tris-HCl, 10 mM $MgCl_2$, 100 μg/mL, pH 7.9), Thermopolis reaction buffer (20 mM Tris-HCl, 10 mM KCl, 10 mM $(NH_4)_2SO_4$, 2 mM $MgSO_4$, 0.1% Triton X-100, pH 8.8) were obtained from New England Biolabs® Inc (Beijing, China). Sodium molybdate dehydrate, L-cysteine, and tetramethylammonium chloride (TMAC) were acquired from Macklin (Shanghai, China). 2-(N-Morpholino) 4-Morpholineethanesulfonic acid (MES), 1 M Tris buffer (pH 8), Tween 20, Ethylenediaminetetraacetic acid disodium salt (EDTA), N-(3-dimethylaminopropyl)-N′-ethylcarbodiimide hydrochloride (EDC) were provided by Aladdin (Shanghai, China). N,N,N′,N′-tetramethylethylenediamine, 30% w/v acrylamide/methylene bisacrylamide (29:1), 5 × TBE, 10% w/v ammonium persulfate, 6 × loading buffer and 4S Red Plus Nucleic Acid Stain were purchased from Sangon Biotech Co., Ltd (Shanghai, China). SYBR Green Iwas obtained from Solarbio (Beijing, China). Methicillin-resistant *Staphylococcus aureus* ATCC 43300 (MRSA), *Staphylococcus aureus* ATCC 29213 (*S. aureus*), *Staphylococcus haemolyticus* ATCC 29970 (*S. haemolyticus*), *Streptococcus pneumoniae* ATCC 49619 (*S. pneumoniae*), *Streptococcus pyogenes* ATCC 19615 (*S. pyogenes*), *Streptococcus mitis* ATCC 49456 (*S. mitis*), *Micrococcus luteus* ATCC 4698 (*M. luteus*), and the clinical strains of MRSA, MDR *Acinetobacter baumannii* (*A. baumannii*), *Mycobacterium tuberculosis* (*M. tuberculosis*), *Pseudomonas aeruginosa* (*P. aeruginosa*), and *Escherichia coli* (*E. coli*) were obtained from Chongqing University Cancer Hospital.

4.2. Preparation of AptMBs and MoS_2 nanosheets

Firstly, magnetic beads (Dynabeads® myone™ carboxylic acid, ThermoFisher Scientific) were characterized by scanning electron microscopy (Hitachi MC1000, Japan) and dynamic light scattering (Malvern Mastersizer 2000, the United Kingdom). Magnetic beads (MBs) were washed with 100 mM MES buffer (pH = 4.8) and re-suspended to a 2 mg/mL concentration in MES buffer. AptMBs were prepared by the condensation reaction of amino-labeled aptamer-blocker duplex and carboxyl-labeled MBs. Specifically, the total reaction volume was 200 μL with 50 μL hybridized products, 1 M EDC, and 1 mg/mL MBs, and the sample was incubated overnight at room temperature on a roller mixer. MBs and AptMBs were analyzed by ultraviolet–visible spectrophotometer (Shimadzu UV-3600, Japan) and vibrating sample magnetometer (quantum design SQUID-VSM, USA).

The hydrothermal method was used to synthesize MoS_2 nanosheets. We have prepared an 80 mL solution (pH 6.5) with 7.5 mg/mL sodium molybdate dehydrate and 10 mg/mL L-cysteine. The solution was stirred vigorously with nitrogen for 1.5 h and reacted in an electric thermostatic drying oven for 48 h at 180°C. After cooling to room temperature, the compounds were washed with anhydrous ethanol three times and freeze-dried for 24 h to obtain MoS_2 nanosheets powder. The obtained MoS_2 was characterized by transmission electron microscopy (FEI Tecnai G2 F30, USA) and X-ray photoelectron spectroscopy (Thermo Fisher Scientific Escalab 250Xi, USA). For X-ray photoelectron spectroscopy (XPS) measurements, the samples were prepared by placing the pre-dried sample powder onto Scotch crystal tape. Monochrome Al-Kα irradiation (1486.6 eV) was used to monitor the chemical composition, and the binding energies were referenced to the adventitious carbon signal at 284.8 eV. The quenching efficiency of MoS_2 nanosheets was characterized by a fluorescence spectrophotometer (Hitachi F-4700, Japan), and the concentrations of each sequence were 0.1 μM, while the concentration of MoS_2 nanosheets was 10 μg/mL.

4.3. Quantitative PCR procedures

Quantification of non-specific and specific amplicons was performed by quantitative PCR (Roche LightCycler 480 II, Switzerland). The PCR mixture for non-specific amplification consists of 400 U/mL Nt. BstNBI, 80 U/mL Vent® (exo-) DNA polymerase, 1 × Thermopol Buffer, 2 mM $MgSO_4$, 100 mM template, 250 μM dNTP, 0.5 × NEB buffer, 1 × SYBR Green I, and a series of concentration of TMAC ranging from 0 mM to 300 mM with a total volume of 50 μL. For specific amplification, 200 mM blockers were included in the PCR mixture. The amplification program included 55°C for 90 min, and the frequency of fluorescence signal collection was 1 min. The qPCR products were further characterized by 12% native polyacrylamide gel electrophoresis. The polyacrylamide gel mixture included 4 mL 30% w/v acrylamide/methylene bisacrylamide (29:1), 2 mL 5 × TBE, 20 μL N,N,N′,N′-tetramethylethylenediamine, 200 μL 10% w/v ammonium persulfate, and distilled water to a final volume of 10 mL. The analytes were incubated in 1 × TBE at 90 mV for 100 min on the Universal Power Supply (Bio-Rad PowerPac™, USA). After that, gels were stained with 4S Red Plus Nucleic Acid Stain and visualized with a ChemDoc™ MP Imaging System (Bio-Rad, USA).

4.4. Bacterial culture and counting

MRSA ATCC 43300, *S. aureus* ATCC 29213, *S. haemolyticus* ATCC 29970, *S. pneumoniae* ATCC 49619, *S. pyogenes* ATCC 19615, *S. mitis* ATCC 49456 and *M. luteus* ATCC 4698 strains were cultured with LB broth. The clinical infection samples of MDR *A. baumannii*, *M. tuberculosis*, *P. aeruginosa* and *E. coli* were grown in their corresponding liquid mediums by inoculating a single colony from the grown

plates, followed by incubation of tubes at 37°C with orbital shaking (200 rpm) for 14–16 h. The bacterial cell growth was estimated as cell turbidity by measuring the optical density at 600 nm ($OD_{600\ nm}$). Bacterial counting was measured by assessing CFU in their corresponding media-agar plates.

4.5. BRICK protocol

The total volume of the conversion system was 20 μL, containing 10^5 CFU MRSA and 0.8 mg/mL AptMBs. The mixture was reacted on a constant temperature shaker for 10 min and separated the supernatant by magnets. Amplification solution included 400 U/mL Nt. BstNBI, 80 U/mL Vent® (exo-) DNA polymerase, 1 × Thermopol Buffer, 2 mM $MgSO_4$, 100 mM template, 250 μM dNTP, 0.5 × NEB buffer, 200 mM TMAC, and separated supernatant with 50 μL of the final volume, and was incubated at 55°C for 60 min in a PCR apparatus (ThermoFisher Scientific SimpliAmp™, USA). After that, a 150 μL separation and reading system containing 100 μM cy5 probes and 5 μg/mL MoS_2 nanosheets was added to the amplification products, and the fluorescence intensity at 668 nm was measured by a fluorescence spectrophotometer (λ_{ex}: 649 nm).

4.6. Ethics statement

All experiments were performed according to relevant guidelines and regulations. bacteria samples used in this study were obtained from the Chongqing University Cancer Hospital, adhering to the institutional ethical standards stipulated in 1964 Helsinki Declaration and its subsequent revisions. Ethical code CZLS2022097-A.

4.7. Statistical analysis

The hybridization temperature between blockers and templates was analyzed by OligoAnalyzer. All statistical tests were analyzed with GraphPad Prism 8.01. The experiments were performed in three biological replicates, and the results are expressed as mean and SD. One-way analysis of variance (ANOVA) was adopted for the comparison of multiple groups with a suitable *post hoc* test. $p < 0.05$ was considered statistically significant.

Credit author statement

Xiaolin Hu: Conceptualization, Methodology, Investigation, Writing – original draft. **Weichao Qin**: Validation, Investigation, Writing – review & editing. **Rui Yuan**: Methodology, Investigation, Writing – review & editing. **Liangliang Zhang**: Methodology. **Liangting Wang**: Methodology. **Ke Ding**: Writing – review & editing. **Ruining Liu**: Writing – review & editing. **Wanyun Huang**: Writing – review & editing. **Hong Zhang**: Conceptualization, Supervision, Writing – review & editing. **Yang Luo**: Conceptualization, Supervision, Writing – review & editing. All authors: Final approval of the manuscript.

Data and materials availability

All data needed to evaluate the conclusions in the paper are present in the paper and/or the Supplementary Materials. Additional data related to this paper may be requested from the authors.

Declaration of competing interest

The authors declare that they have no known competing financial interests or personal relationships that could have appeared to influence the work reported in this paper.

Acknowledgments

This work was supported by the National Key Research and Development Program (Grant No. 2022YFC2009603), National Natural Science Foundation of China (Grant Nos. 82125022, 82072383), the Key Natural Science Foundation of Chongqing (Grant Nos. CSTC2020JCYJ-ZDXMX0006, CSTC2020JSCX-CYLHX0001), the Chongqing medical scientific research project (Joint project of Chongqing Health Commission and Science and Technology Bureau) (Grant No. 2020FYYX018), the Fundamental Research Funds for the Central Universities (Grant No. 2022CDJQY-002), Chongqing Returned Overseas Students' Entrepreneurship and Innovation Support Program (Grant No. CX2021010), Postdoctoral Innovation Talents Support Program (Grant No. BX20220194).

Appendix A. Supplementary data

Supplementary data to this article can be found online at https://doi.org/10.1016/j.mtbio.2022.100379.

References

[1] T. Thompson, The staggering death toll of drug-resistant bacteria, Nature (2022), https://doi.org/10.1038/d41586-022-00228-x.
[2] J.A. Jernigan, K.M. Hatfield, H. Wolford, R.E. Nelson, B. Olubajo, S.C. Reddy, N. McCarthy, P. Paul, L.C. McDonald, A. Kallen, A. Fiore, M. Craig, J. Baggs, Multidrug-resistant bacterial infections in US hospitalized patients, 2012-2017, N. Engl. J. Med. 382 (14) (2020) 1309–1319.
[3] D.G.J. Larsson, C.F. Flach, Antibiotic resistance in the environment, Nat. Rev. Microbiol. 20 (2022) 257–269.
[4] G. Qing, X. Zhao, N. Gong, J. Chen, X. Li, Y. Gan, Y. Wang, Z. Zhang, Y. Zhang, W. Guo, Y. Luo, X.J. Liang, Thermo-responsive triple-function nanotransporter for efficient chemo-photothermal therapy of multidrug-resistant bacterial infection, Nat. Commun. 10 (1) (2019) 4336.
[5] B.M. Kuehn, Alarming antimicrobial resistance trends emerge globally, JAMA, J. Am. Med. Assoc. 324 (3) (2020) 223.
[6] K. O'Leary, The global burden of antimicrobial resistance, Nat. Med. (2022), https://doi.org/10.1038/d41591-022-00033-z.
[7] J. Dietvorst, L. Vilaplana, N. Uria, M.P. Marco, X. Munoz-Berbel, Current and near-future technologies for antibiotic susceptibility testing and resistant bacteria detection, Trac-Trend. Anal. Chem. 127 (2020), 115891.
[8] M.I. Villalba, P. Stupar, W. Chomicki, M. Bertacchi, G. Dietler, L. Arnal, M.E. Vela, O. Yantorno, S. Kasas, Nanomotion detection method for testing antibiotic resistance and susceptibility of slow-growing bacteria, Small 14 (4) (2018), 1702671.
[9] V. Vedarethinam, L. Huang, W. Xu, R. Zhang, D.D. Gurav, X.M. Sun, J. Yang, R.P. Chen, K. Qian, Detection and inhibition of bacteria on a dual-functional silver platform, Small 15 (3) (2019), 1803051.
[10] M.S. Lee, H. Hyun, I. Park, S. Kim, D.H. Jang, S. Kim, J.K. Im, H. Kim, J.H. Lee, T. Kwon, J.H. Kang, Quantitative fluorescence in situ hybridization (FISH) of magnetically confined bacteria enables early detection of human bacteremia, Small Methods 6 (2022), 2101239.
[11] W. Zhao, M. Ding, X. Zhang, Z.R. Xin, L.J. Song, Z.Y. Cheng, S.F. Luan, Metabolism-driven disassembly of nanoprobes for bacterial detection, imaging, and photo-inactivation, Adv. Funct. Mater. 32 (2021), 2107574.
[12] L. Xu, W. Liang, Y.L. Wen, L.L. Wang, X. Yang, S.Z. Ren, N.Q. Jia, X.L. Zuo, G. Liu, An ultrasensitive electrochemical biosensor for the detection of mecA gene in methicillin-resistant Staphylococcus aureus, Biosens. Bioelectron. 99 (2018) 424–430.
[13] Y.X. Zhai, X.Y. Zhu, B.N. Xu, Y. Wang, Dual-labeling ratiometric electrochemical strategy initiated with ISDPR for accurate screening MecA gene, Biosens. Bioelectron. 197 (2022), 113772.
[14] J. Zhou, R.J. Fu, H.R. Liu, Y.L. Liu, Y.W. Wang, B.N. Jiao, Y. He, H.W. Tang, Integrating multiple hybridization chain reactions on gold nanoparticle and alkaline phosphatase-mediated in situ growth of gold nanobipyramids: an ultrasensitive and high color resolution colorimetric method to detect the mecA gene of Staphylococcus aureus, J. Hazard Mater. 418 (2021), 126223.
[15] I. Choopara, A. Suea-Ngam, Y. Teethaisong, P.D. Howes, M. Schmelcher, A. Leelahavanichkul, S. Thunyaharn, D. Wongsawaeng, A.J. DeMello, D. Dean, N. Somboonna, Fluorometric paper-based, loop-mediated isothermal amplification devices for quantitative point-of-care detection of methicillin-resistant Staphylococcus aureus (MRSA), ACS Sens. 6 (3) (2021) 742–751.
[16] M.A.A. Mohamed, H.N. Kozlowski, J. Kim, K. Zagorovsky, M. Kantor, J.J. Feld, S. Mubareka, T. Mazzulli, W.C.W. Chan, Diagnosing antibiotic resistance using nucleic acid enzymes and gold nanoparticles, ACS Nano 15 (6) (2021) 9379–9390.
[17] P. Athamanolap, K. Hsieh, L.B. Chen, S. Yang, T.H. Wang, Integrated bacterial identification and antimicrobial susceptibility testing using PCR and high-resolution melt, Anal. Chem. 89 (21) (2017) 11529–11536.

[18] R. Yuan, W.Y. Tang, H. Zhang, W.X. You, X.L. Hu, H.W. Zhang, L. Chen, W.Q. Nian, S.J. Ding, Y. Luo, Palindromic-assisted self-annealing transcription amplification for reliable genotyping of epidermal growth factor receptor exon mutations, Biosens. Bioelectron. 194 (2021), 113633.
[19] A. Patino Diaz, S. Bracaglia, S. Ranallo, T. Patino, A. Porchetta, F. Ricci, Programmable cell-free transcriptional switches for antibody detection, J. Am. Chem. Soc. 144 (13) (2022) 5820–5826.
[20] L. Mou, H.H. Hong, X.J. Xu, Y. Xia, X.Y. Jiang, Digital hybridization human papillomavirus assay with attomolar sensitivity without amplification, ACS Nano 15 (8) (2021) 13077–13084.
[21] W.P. Peng, Y. Qin, W.N. Li, M.H. Chen, D.M. Zhou, H.X. Li, J.Y. Cui, J. Chang, S. Xie, X.Q. Gong, B.Z. Tang, Nonenzyme cascaded amplification biosensor based on effective aggregation luminescence caused by disintegration of silver nanoparticles, ACS Sens. 5 (7) (2020) 1912–1920.
[22] H. Zhang, R. Liu, Q. Li, X. Hu, L. Wu, Y. Zhou, G. Qing, R. Yuan, J. Huang, W. Gu, Y. Ye, C. Qi, M. Han, X. Chen, X. Zhu, Y. Deng, L. Zhang, H. Chen, H. Zhang, W. Gao, Y. Liu, Y. Luo, Flipped quick-response code enables reliable blood grouping, ACS Nano 15 (4) (2021) 7649–7658.
[23] A.R. Chandrasekaran, J.A. Punnoose, L. Zhou, P. Dey, B.K. Dey, K. Halvorsen, DNA nanotechnology approaches for microRNA detection and diagnosis, Nucleic Acids Res. 47 (20) (2019) 10489–10505.
[24] X.X. Zhao, L.L. Zeng, Q. Mei, Y. Luo, Allosteric probe-initiated wash-free method for sensitive extracellular vesicle detection through dual cycle-assisted CRISPR-cas12a, ACS Sens. 5 (7) (2020) 2239–2246.
[25] R. Yuan, X. Bai, X. Hu, H. Zhang, C. Hou, Q. Long, Y. Luo, CATCH: high specific transcriptome-focused fusion gene variants discrimination, Chem. Commun. 58 (55) (2022) 7618–7621.
[26] E.M. McConnell, J. Nguyen, Y. Li, Aptamer-based biosensors for environmental monitoring, Front. Chem. 8 (2020) 434.
[27] K. Wang, B.S. He, L.L. Xie, L.P. Li, J.P. Yang, R.L. Liu, M. Wei, H.L. Jin, W.J. Ren, Exonuclease III-assisted triple-amplified electrochemical aptasensor based on PtPd NPs/PEI-rGO for deoxynivalenol detection, Sensor. Actuat. B-Chem. 349 (2021), 130767.
[28] X.Y. Yang, L.H. Wang, L.D. Pang, S.Q. Fu, X. Qin, Q. Chen, C.X. Man, Y.J. Jiang, A novel fluorescent platform of DNA-stabilized silver nanoclusters based on exonuclease III amplification-assisted detection of Salmonella Typhimurium, Anal. Chim. Acta 1181 (2021), 338903.
[29] J.G. Carter, L.O. Iturbe, J.L.H.A. Duprey, I.R. Carter, C.D. Southern, M. Rana, C.M. Whalley, A. Bosworth, A.D. Beggs, M.R. Hicks, J.H.R. Tucker, T.R. Dafforn, Ultrarapid detection of SARS-CoV-2 RNA using a reverse transcription-free exponential amplification reaction, RTF-EXPAR, Proc. Natl. Acad. Sci. USA 118 (35) (2021), e2100347118.
[30] J.F. Qian, T.M. Ferguson, D.N. Shinde, A.J. Ramirez-Borrero, A. Hintze, C. Adami, A. Niemz, Sequence dependence of isothermal DNA amplification via EXPAR, Nucleic Acids Res. 40 (11) (2012) e87.
[31] M.S. Reid, X.C. Le, H.Q. Zhang, Exponential isothermal amplification of nucleic acids and assays for proteins, cells, small molecules, and enzyme activities: an EXPAR example, Angew. Chem., Int. Ed. 57 (37) (2018) 11856–11866.
[32] N.V. Zyrina, V.N. Antipova, Nonspecific synthesis in the reactions of isothermal nucleic acid amplification, Biochemistry-Moscow+ 86 (7) (2021) 887–897.
[33] J.K. Mao, S.Y. Tang, S.J. Liang, W.F. Pan, Y.L. Kang, J.B. Cheng, D.D. Yu, J. Chen, J.A. Lou, H. Zhao, J.G. Zhou, A new self-passivating template with the phosphorothioate strategy to effectively improve the detection limit and applicability of exponential amplification reaction, Anal. Methods-Uk 13 (35) (2021) 3947–3953.
[34] G. Gines, R. Menezes, K. Nara, A.S. Kirstetter, V. Taly, Y. Rondelez, Isothermal digital detection of microRNAs using background-free molecular circuit, Sci. Adv. 6 (4) (2020), eaay5952.
[35] J.P. Wang, B.J. Zou, J.Z. Rui, Q.X. Song, T. Kajiyama, H. Kambara, G.H. Zhou, Exponential amplification of DNA with very low background using graphene oxide and single-stranded binding protein to suppress non-specific amplification, Microchim. Acta 182 (5–6) (2015) 1095–1101.
[36] M.S. Reid, R.E. Paliwoda, H.Q. Zhang, X.C. Le, Reduction of background generated from template-template hybridizations in the exponential amplification reaction, Anal. Chem. 90 (18) (2018) 11033–11039.
[37] J. Chen, X.Q. Zhou, Y.J. Ma, X.L. Lin, Z. Dai, X.Y. Zou, Asymmetric exponential amplification reaction on a toehold/biotin featured template: an ultrasensitive and specific strategy for isothermal microRNAs analysis, Nucleic Acids Res. 44 (15) (2016) e130.
[38] V.V. Singh, K. Kaufmann, B.E.F. de Avila, E. Karshalev, J. Wang, Molybdenum disulfide-based tubular microengines: toward biomedical applications, Adv. Funct. Mater. 26 (34) (2016) 6270–6278.
[39] M. Kukkar, G.C. Mohantaa, S.K. Tuteja, P. Kumar, A.S. Bhadwal, P. Samaddar, K.H. Kim, A. Deep, A comprehensive review on nano-molybdenum disulfide/DNA interfaces as emerging biosensing platforms, Biosens. Bioelectron. 107 (2018) 244–258.
[40] A.H. Loo, A. Bonanni, A. Ambrosi, M. Pumera, Molybdenum disulfide (MoS_2) nanoflakes as inherently electroactive labels for DNA hybridization detection, Nanoscale 6 (20) (2014) 11971–11975.
[41] C.F. Zhu, Z.Y. Zeng, H. Li, F. Li, C.H. Fan, H. Zhang, Single-layer MoS_2-based nanoprobes for homogeneous detection of biomolecules, J. Am. Chem. Soc. 135 (16) (2013) 5998–6001.
[42] D. Zhu, J. Huang, B. Lu, Y. Zhu, Y. Wei, Q. Zhang, X. Guo, L. Yuwen, S. Su, J. Chao, L. Wang, Intracellular MicroRNA imaging with MoS_2-supported nonenzymatic catassembly of DNA hairpins, ACS Appl. Mater. Interfaces 11 (23) (2019) 20725–20733.
[43] G. Oudeng, M. Benz, A.A. Popova, Y. Zhang, C.Q. Yi, P.A. Levkin, M. Yang, Droplet microarray based on nanosensing probe patterns for simultaneous detection of multiple HIV retroviral nucleic acids, ACS Appl. Mater. Interfaces 12 (50) (2020) 55614–55623.
[44] L. Kong, X. Zhou, G. Shi, Y. Yu, Molybdenum disulfide nanosheets-based fluorescent "off-to-on" probe for targeted monitoring and inhibition of beta-amyloid oligomers, Analyst 145 (19) (2020) 6369–6377.
[45] M.L. Gao, F. He, B.C. Yin, B.C. Ye, A dual signal amplification method for exosome detection based on DNA dendrimer self-assembly, Analyst 144 (6) (2019) 1995–2002.
[46] X.X. Zhao, W.Q. Zhang, X.P. Qiu, Q. Mei, Y. Luo, W.L. Fu, Rapid and sensitive exosome detection with CRISPR/Cas12a, Anal. Bioanal. Chem. 412 (3) (2020) 601–609.